Rab11a mediates cell-cell spread and reassortment of influenza A virus genomes via tunneling nanotubes.

Ketaki Ganti[1], Julianna Han[2#], Balaji Manicassamy[2], Anice C. Lowen[1, 3*]*

1 Department of Microbiology and Immunology, Emory University School of Medicine, Atlanta, GA, USA

2 Department of Microbiology and Immunology, University of Iowa School of Medicine, Iowa City, IA

3 Emory-UGA Centers of Excellence for Influenza Research and Surveillance (CEIRS)

Current address: Department of Integrative Structural and Computational Biology, The Scripps Research Institute, La Jolla, CA, USA

*Corresponding Authors

Email: ketaki.ganti@emory.edu; anice.lowen@emory.edu

Abstract:

Influenza A virus (IAV) genomes comprise eight negative strand RNAs packaged into virions in the form of viral ribonucleoproteins (vRNPs). Rab11a plays a crucial role in the transport of vRNPs from the nucleus to the plasma membrane via microtubules, allowing assembly and virus production. Here, we identify a novel function for Rab11a in the inter-cellular transport of IAV vRNPs using tunneling nanotubes (TNTs) as molecular highways. TNTs are F-Actin rich tubules that link the cytoplasms of nearby cells. In IAV-infected cells, Rab11a was visualized together with vRNPs in these actin-rich intercellular connections. To better examine viral spread via TNTs, we devised an infection system in which conventional, virion-mediated, spread was not possible. Namely, we generated HA-deficient reporter viruses which are unable to produce progeny virions but whose genomes can be replicated and trafficked. In this system, vRNP transfer to neighboring cells was observed and this transfer was found to be dependent on both actin and Rab11a. Generation of infectious virus via TNT transfer was confirmed using donor cells infected with HA-deficient virus and recipient cells stably expressing HA protein. Mixing donor cells infected with genetically distinct IAVs furthermore revealed the potential for Rab11a and TNTs to serve as a conduit for genome mixing and reassortment in IAV infections. These data therefore reveal a novel role for Rab11a in the IAV life cycle, which could have significant implications for within-host spread, genome reassortment and immune evasion.

Author Summary:

Influenza A viruses infect epithelial cells of the upper and lower respiratory tract in humans. Infection is propagated by the generation of viral particles from infected cells, which disseminate within the tissue. Disseminating particles can encounter obstacles in the extracellular environment, including mucus, ciliary movement, antibody neutralization and uptake by phagocytic immune cells. An alternative mode of spread, which avoids these hazards, involves direct transport of viral components between cells. This cell-cell spread of infection is not a well understood process. In this study we demonstrate that the host factor Rab11a mediates the transport of viral genomes in the cell-cell spread of infection. Rab11a is already known to play a pro-viral role in the transport of viral genomes to the plasma membrane for assembly into virus particles. Here, we see that this same transport mechanism is co-opted for direct cell-cell spread through cellular connections called tunneling nanotubes. We show that complexes of Rab11a and viral components can be trafficked across tunneling nanotubes, transmitting infection without the formation of virus particles. Importantly, this route of spread often seeds viral genomes from multiple donor cells into recipient cells, which in turn increases viral genetic diversity.

Introduction:

Influenza A virus (IAV) genomes are comprised of eight RNA segments that are packaged into the virion in the form of viral ribonucleoproteins (vRNPs), which contain viral nucleoprotein (NP) as well as the polymerase complex (PB2, PB1 and PA) (1). Influenza genome packaging mechanisms

have been studied extensively and, although there are a lot of unknowns, it has been demonstratively shown that the host cell protein Rab11a is crucial for the trafficking of newly synthesized vRNPs after they exit the nucleus to the site of assembly at the plasma membrane (2). Rab11a is a small GTPase that has multiple roles in the host cell, including a pivotal role in retrograde transport of cargo on recycling endosomes (3,4). The intracellular transport of vRNP-Rab11a complexes is thought to occur via the microtubule network with the help of dynein motors (5–8), and disruption of this network by nocodazole has been shown to attenuate the generation of viral progeny (5). Similarly, our work has shown that loss of Rab11a also leads to a reduction in viral titer, most likely due to a defect in the packaging of vRNPs, leading to the formation of incomplete viral particles (unpublished). Taken together, these data demonstrate the importance of an intact microtubule network as well as Rab11a in the influenza virus life cycle.

Tunneling nanotubes (TNTs) are F-Actin rich cellular connections that are formed between two or more cells (9). These connections can be formed over long distances and provide cytoplasmic connectivity between the cells, allowing for exchange of materials including organelles, nutrients, and membrane vesicles (10–12). Many viruses including HIV (13–15), herpesviruses (16) and influenza A viruses (17,18) have been shown to utilize these TNTs for cell-cell spread. Previous work by Roberts et al. and Kumar et al. has shown that influenza A virus spread via TNTs proceeds even in the presence of neutralizing antibodies or antivirals such as oseltamivir (17,18). This mode of infection does not depend on the formation of viral particles, thus allowing for the assembly stage of the lifecycle to be bypassed. Although the use of TNTs by IAVs has been shown, the exact mechanism is unclear.

In this study, we show that Rab11a mediates the transport of IAV vRNPs and proteins through TNTs, as evidenced by Rab11a co-localization with viral components in TNTs and the disruption of this transport with Rab11a knock out. This system was observed to be functional in multiple host cell backgrounds and virus strains. Using HA deficient viruses, we confirm that transport of viral components through TNTs can seed productive infection in recipient cells. In the context of viral co-infection, we find direct cell-cell spread often seeds viral genomes from multiple donor cells into recipient cells, thus promoting genome mixing and reassortment. Finally, our data suggests that, at least in the case of IAV infection, TNTs access the cytosol of both connected cells and allow bi-directional movement of cargo. Taken together, these findings demonstrate a novel and crucial role for Rab11a in the trafficking of IAV genomes via tunneling nanotubes and extend mechanistic understanding of this unconventional mode of viral dissemination.

Results:

IAV vRNPs associate with Rab11a within F-Actin rich TNTs.

Upon nuclear exit, IAV vRNPs bind to Rab11a via PB2, allowing their transport to the plasma membrane for assembly. We hypothesized that vRNP-Rab11a complexes could also be routed to F-Actin rich intercellular connections called tunneling nanotubes (TNTs) and could seed new infections by direct transport through TNTs. To test this hypothesis, we visualized Rab11a, F-Actin and viral nucleoprotein (NP) - as a marker for vRNPs - in MDCK cells infected with either influenza A/Netherlands/602/2009 (NL09; pH1N1) or A/Panama/2007/99 (P99; H3N2) virus. NP and Rab11a were seen to co-localize in a perinuclear compartment, as has been shown previously (2,8). In addition, co-localization of these components was observed within the F-Actin rich TNTs

104 connecting infected and uninfected cells (Fig 1A). This observation suggests that there are at least
105 two functional pathways for the trafficking of vRNP-Rab11a complexes post nuclear exit: the
106 canonical assembly pathway and the TNT-mediated genome transfer pathway.

107 To further corroborate the role of Rab11a in the transport of vRNPs across TNTs, we utilized
108 Rab11a knockout (KO) A549 cells generated by CRISPR/Cas9 and wild type (WT) A549 cells as a
109 control. As before, cells were infected with either NL09 or P99 viruses and then stained for NP,
110 Rab11a and F-Actin. WT cells showed co-localization of NP and Rab11a in the perinuclear region
111 and within TNTs (Fig 1B and Supp Fig 1). Conversely, Rab11a KO cells did not show NP staining
112 within the TNTs, indicating that Rab11a drives the transfer of vRNPs through TNTs (Fig 1C and
113 Supp Fig 1).

114 ***Disruption of actin or loss of Rab11a significantly attenuates direct cell-cell transmission of***
115 ***infection****.*

116 Since we observed the presence of vRNP-Rab11a complexes within TNTs, we next tested whether
117 the loss of either the TNTs or Rab11a influences the cell-cell spread of IAV infection. Previously,
118 neutralizing antibodies or neuraminidase inhibitors have been used to block conventional viral
119 infection and allow examination of IAV protein and RNA transport via TNTs (17,18). Although
120 these methods are effective in abrogating conventional spread, we wanted to fully eliminate the
121 generation of viral progeny to define the role of Rab11a and TNTs in IAV genome transfer more
122 clearly. To this end, we rescued recombinant viruses in the NL09 and P99 strain backgrounds that
123 lack the HA gene but instead contain either mVenus (NL09 ΔHA Venus; P99 ΔHA Venus) or
124 mScarlet (NL09 ΔHA Scarlet) fluorescent reporter ORFs flanked by HA packaging signals. These

125 HA deficient reporter viruses are infection competent but are unable to produce progeny in the
126 absence of a HA complementing cell line. Therefore, these viruses are excellent tools to study
127 the cell-cell spread of IAV infection via TNTs.

128 To analyze the role of F-actin in the cell-cell spread of viral genomes, MDCK cells were infected
129 with either NL09 ΔHA Venus or P99 ΔHA Venus viruses in the presence or absence of Cytochalasin
130 D, which is a potent inhibitor of actin polymerization and disrupts TNTs (17,18). Cytochalasin D
131 was added 2 h post internalization. HA positive cells were counted at 16, 24, and 48 h post-
132 infection (p.i) and binned into one of two categories: single cells or foci comprising >=2
133 contiguous, positive cells. We hypothesized that the disruption of TNTs by Cytochalasin D would
134 severely limit the spread of IAV genomes from infected cells, preventing the formation of infected
135 foci. As shown in Figure 2, there was a significant reduction in the number of infected foci in the
136 Cytochalasin D treated cells compared to the untreated controls in both the NL09 ΔHA Venus and
137 P99 ΔHA Venus infected cells. These data confirm that intact TNTs are required for direct cell-cell
138 spread of IAV genetic material.

139 Next, we analyzed the role of Rab11a in direct cell-cell spread of IAV. To do this, A549 WT and
140 Rab11a KO cells were infected with either NL09 ΔHA Venus or P99 ΔHA Venus viruses. Venus
141 positive cells were counted at 16, 24, and 48 h p.i. and categorized based on their presence as
142 single cells or within foci at each time point. If Rab11a directs transport of vRNPs across TNTs,
143 the loss of Rab11a would be expected to reduce the cell-cell spread of IAV genetic material. As
144 shown Figure 3, this is indeed the case. In contrast to WT controls, the number of infected foci
145 did not increase over time in the Rab11 KO cells. These data provide further evidence for the role
146 of Rab11a in this alternate infection pathway.

Virion-independent genome transfer leads to productive infection by an actin-dependent mechanism.

To assess whether all eight genome segments can be transported via TNTs leading to the production of infectious progeny, we performed a co-culture experiment using MDCK cells and a MDCK-derived cell line which expresses the HA of influenza A/WSN/33 (H1N1) virus on the cell surface (MDCK WSN HA cells). When infected with an HA deficient reporter virus, these cells provide the HA protein required for the generation of infectious virus particles. For subsequent analysis of co-infection via TNT/Rab11a mediated genome transfer, these experiments were set up using two IAV strains, NL09 ΔHA Venus WT and NL09 ΔHA Scarlet VAR viruses. In addition to carrying differing reporter genes, these differ in the presence of a silent mutation in each segment of the VAR virus, which acts as a genetic tag (19). Neither of these differences is important for the purposes of the present analysis.

As outlined in Figure 4A, separate dishes of MDCK cells were singly infected with either NL09 ΔHA Venus WT or NL09 ΔHA Scarlet VAR virus, each at a MOI of 25 or 2.5 PFU/cell. After infection for 2 hours, the cells were acid washed to remove residual inoculum and then trypsinized to make a cell slurry. MDCK cells infected with NL09 ΔHA Venus WT and NL09 ΔHA Scarlet VAR were mixed with naïve MDCK WSN HA cells in the ratio 1:1:2. The cell mixture was plated in medium containing trypsin (to allow activation of HA) and ammonium chloride (to prevent secondary infections mediated by virus particles). The cells were also treated with either vehicle or 30 µM Cytochalasin D. If all eight segments of the viral genome can be transported across TNTs to a conducive cell, which in this case must be a MDCK WSN HA cell, then the recipient cell will produce virus particles. To detect any such progeny viruses produced, supernatant was collected

at 24, 48 and 72 h post mixing and plaque assays were performed on MDCK WSN HA cells. As can be seen from Figure 4B infectious virus was detected in the vehicle treated control cells, but not in the Cytochalasin D treated cells. Virus production in vehicle treated cells demonstrates the transfer of the full complement of IAV genome segments from infected cells which lack HA protein and cannot produce virions to cells which express complementing HA protein. A lack of virus production in Cytochalasin D treated cells indicates that this transfer was TNT-dependent. Comparing the two MOIs tested, a dose dependence was observed at 24 h, which is most likely due to the increased probability of an infected cell making a connection with a naïve MDCK WSN HA cell at higher MOI.

To analyze the effect of the loss of Rab11a on the production of infectious progeny, we co-cultured either A549 WT or A549 Rab11a KO cells infected with the NL09 ΔHA Venus WT or NL09 ΔHA Scarlet VAR viruses with the MDCK WSN HA complementing line as described above. Supernatant was collected at 24, 48 and 72 h post mixing and plaque assays were performed on MDCK WSN HA cells. As can be seen from Figure 4C, infectious virus was detected from both A549 WT and Rab11a KO cells, with a marginal difference in titers. Since this observation was incongruent with our previous data demonstrating the importance of Rab11a in the transport of vRNPs, we hypothesized the transfer of viral genomes from the Rab11a KO cells was occurring via Rab11a that originates in the MDCK WSN HA cells. If correct, this observation would indicate that TNTs are open ended and allow for bi-directional movement of cargo.

TNTs allow bidirectional shuttling of Rab11a between cells

To analyze if Rab11a could shuttle from one cell to another in a bi-directional manner, we used A549 cells stably expressing Rab11a fused to an mCherry fluorescent reporter in combination with A549 Rab11a KO cells. Briefly, A549 Rab11a KO cells were infected with NL09 WT virus at a MOI of 25. After 2 hours, the cells were acid washed to remove residual inoculum and then trypsinized to make a cell slurry. The infected cells were then mixed with uninfected A549 mCherry Rab11a cells in a 1:1 ratio and plated onto coverslips, in the presence of vehicle or Cytochalasin D. At 24 h post mixing, cells were stained to visualize NP and F-Actin. As can be seen in Figure 5 and Supplementary Figure 2, in the absence of Cytochalasin D we observe co-localization of Rab11a and NP in the A549 Rab11 KO cells, indicating the transfer of mCherry Rab11a to the infected cells. The cells treated with Cytochalasin D do not show such co-localization, further demonstrating the crucial role of an intact F-Actin structure. These data thus show that the TNTs formed between cells in IAV infections are open ended and allow bi-directional movement.

TNTs serve as conduits for genome mixing and reassortment.

Since we observed that infectious progeny could be generated via Rab11a-mediated genome transfer through TNTs, we hypothesized that this process could also mediate co-infection and therefore reassortment. In particular, reassortment would be expected if differentially infected donor cells connect to the same recipient cell. To test this hypothesis, the genotypes of virus produced from the co-cultures described in Figure 4B were evaluated. In these experiments, cells infected with NL09 ΔHA Venus WT virus were mixed with cells infected with NL09 ΔHA Scarlet VAR virus and these infected cells were in turn mixed with MDCK WSN HA cells; thus, co-infections could occur if WT infected and VAR infected cells each formed connections with the

same HA-expressing recipient cell and a full complement of IAV segments was reconstituted therein. The silent mutations differentiating each of the non-HA gene segments of the WT and VAR viruses allow the parental origin of segments to be identified. Thus, to evaluate reassortment, plaque clones were isolated from co-culture supernatants and the genotype of each was determined. The results show that viruses generated from MDCK WSN HA cells mixed with infected A549 WT cells were predominantly reassortant under all conditions evaluated (Figure 6A). In contrast, when MDCK WSN HA cells were mixed with infected A549 Rab11 KO cells, parental viruses typically dominated (Figure 6B). Thus, in a Rab11a-sufficient system, intercellular transfer of IAV vRNPs through TNTs readily yielded reassortants, indicating that TNTs are forming a network rather than pairwise connections between cells. When Rab11a was absent from infected donor cells, however, reassortants were rarely observed, suggesting that either fewer TNT connections are formed or vRNP transport through TNTs is less efficient.

We note that in both data sets shown in Figure 6, richness of viral genotypes was low, with at most four distinct gene constellations detected in each sample of 21 plaque isolates. This observation suggests that very few cells are producing most of the progeny virus in this experimental system, and that each producer cell is releasing virus with only one or a small number of genotypes. In turn, this suggests that MDCK WSN HA cells that receive a full complement of IAV vRNPs do not tend to receive multiple copies of a given segment. Although low in both culture systems, richness was significantly higher in the samples derived from A549 WT cells compared to those from A549 Rab11a KO cells, with 2.8 and 1.9 unique genotypes detected on average, respectively ($p=0.019$, t-test). This difference is consistent with less efficient vRNP transfer when donor cells lack Rab11a.

Discussion:

Our data reveal a novel role for the host GTPase Rab11a in the trafficking of IAV genomes via tunneling nanotubes. We decisively show that productive infection can be mediated through this direct cell-to-cell route and find evidence that Rab11a can move through TNTs in a bidirectional manner to mediate IAV genome transfer. In the context of mixed infections, we furthermore find that TNT/Rab11a-mediated transfer readily leads to cellular coinfection and reassortment.

The trafficking of IAV genomes is a complex and poorly understood process. Although it is known that newly synthesized vRNPs form transient complexes with active Rab11a post nuclear exit and are trafficked to the plasma membrane for assembly on microtubule structures (5–8), the fate of these complexes is not completely elucidated. Here we examined the potential for Rab11a-vRNP complexes to be trafficked through TNTs to neighboring cells. Tunneling nanotubes (TNTs) are F-Actin based cytoplasmic connections that are utilized for long distance communication and have been shown to have a role in the IAV life cycle (17,18). TNTs can be used to transport vesicular cargo (10,20–22), so we posed the question of whether the Rab11a-vRNP vesicular complexes could be re-routed to these structures. We show that Rab11a and vRNPs co-localize within TNTs in multiple cell types. Loss of Rab11a leads to severely reduced detection of NP within the TNTs and dispersed NP localization within the cytoplasm. These observations strongly suggest that Rab11a-vRNP complexes are transported within TNTs.

TNTs are mainly composed of F-Actin and the transport of organelles through TNTs requires myosin motor activity on actin filaments (11,23–25). Since Rab11a can utilize both dynein motors, which drive microtubule movement (6,26,27), and myosin motors, which drive actin dynamics

(28–30), the observation that Rab11a mediates transport through TNTs raises the question of which motor proteins are involved. Studies to date on IAV infection have mainly focused on the role of Rab11a and microtubules. Further studies are needed to determine whether the same transport mechanism is active within TNTs and whether Rab11a-actin dynamics may function in vRNP transport both within and between cells.

The observation that infectious progeny could be recovered from co-cultures of infected Rab11a KO A549 cells with MDCK WSN HA cells, appeared to indicate that Rab11a is not required to mediate transport of vRNPs through TNTs. However, this observation made in the context of co-culture was reconciled with results from Rab11a KO A549 cell mono-culture by the visualization of mCherry Rab11a within infected Rab11a KO cells. TNTs can be formed in multiple ways - single ended, open ended or closed - and therefore support varying modes of transport (9,12,31). Our experiments were dependent on an HA-encoding producer cell that expresses functional Rab11a. As a result, the generation of progeny virions in the Rab11a KO co-culture is likely due to the formation of open ended, bi-directional TNTs that allow Rab11a from the producer cell to shuttle to and from infected KO cells where it could pick up vRNPs. This process seems to be inefficient, however, as evidenced by the low rate of reassortment observed when infected cells do not encode Rab11a. The possibility of bidirectional trafficking of vRNPs between cells opens hitherto unexplored avenues of viral infection.

Our data revealing that coinfection and reassortment can occur through TNT transfer of vRNPs between cells raise new questions about the processes driving IAV genetic exchange. The prevalence of reassortants produced via TNT transfer from Rab11a+ cells indicates that vRNPs may be trafficked individually or as subgroups and not as a constellation of 8 segments. This

process would then seed incomplete viral genomes into recipient cells, which require complementation to allow the production of progeny viruses. Owing to this reliance on complementation, incomplete viral genomes are known to augment reassortment (32–34). Our data suggest that both seeding and complementation of incomplete viral genomes can occur via TNT transfer of vRNPs. In the presence of a conventional viral infection system, co-infection with multiple virions is thought to be the *modus operandi* of IAV reassortment, where reassortment efficiency is a function of the dose and relative timing of two infections, as well as levels of incomplete viral genomes (19,32). It will be interesting to determine whether TNT-mediated co-infection is also sensitive to dose and timing. More broadly, further work is needed to tease out the extent to which TNT mediated reassortment occurs alongside conventional modes of reassortment.

IAV spread through TNTs may be particularly important in the evasion of antibodies, and other antiviral factors that act directly on extracellular virions, in a manner that does not depend on the generation of escape mutants. Direct cell-cell spread may also make an important contribution to spatial structure within the infected host, leading to more localized spread and limiting mixing among *de novo* variants (35). To further investigate these potential implications, an exciting prospect for future work is the development of *ex vivo* and *in vivo* models for the study and visualization of TNT mediated cell-cell spread.

In summary, our data show a novel role for Rab11a in the IAV life cycle, where it can mediate vesicular transport of vRNPs across TNTs and seed new infections (Figure 7). Future work to elucidate the exact mechanism of transport of the Rab11a-vRNP complexes, including the motors

297 utilized and the fate of the incoming Rab11a-vRNP complexes in the recipient cytosol, are exciting
298 avenues to be studied and will further our understanding of IAV-host interactions.

299 **Materials and Methods:**

300 *Cells and cell culture media*

301 MDCK cells (obtained from Dr. Daniel Perez) and MDCK WSN HA cells (obtained from Dr. Ryan
302 Langlois) were maintained Minimal Essential Medium (Sigma) supplemented with 10% fetal
303 bovine serum (FBS; Atlanta Biologicals), penicillin (100 IU ml^{-1}), and streptomycin (100 µg ml^{-1};
304 PS; Corning). A549 WT, A549 Rab11a KO and A549 mCherry Rab11a (6) (obtained from Dr. Seema
305 Lakdawala) were maintained in Dulbecco's Modified Essential Medium (Gibco) supplemented
306 with 10% FBS (Atlanta Biologicals), and PS. All cells were cultured at 37 °C and 5% CO_2 in a
307 humidified incubator. All cell lines were tested monthly for mycoplasma contamination while in
308 use. The medium for culture of IAV in each cell line (termed virus medium) was prepared by
309 eliminating FBS and supplementing the appropriate medium with 4.3% BSA and PS. Ammonium
310 chloride-containing virus medium was prepared by the addition of HEPES buffer and NH_4Cl at
311 final concentrations of 50 mM and 20 mM, respectively. OPTi-MEM (Gibco) was used as a serum
312 free medium where indicated.

313 *Generation of CRISPR KO Cells*

314 Rab11a KO A549 cells were generated using two guide RNAs (gRNA) targeting the promoter and
315 exon 1 of the Rab11a gene as previously described (36). Oligonucleotides for the CRISPR target
316 sites T1 (forward CACCGCATTTCGAGTAAATCGAGAC and reverse
317 AAACGTCTCGATTTACTCGAAATGC) and T2 (forward CACCGTAACATCAGCGTAAGTCTCA and

reverse AAACTGAGACTTACGCTGATGTTAC) were annealed and cloned into lentiCRISPRv2 (Addgene #52961) and LRG (Addgene #65656) expression vectors, respectively. A549 cells transduced with lentivirus vectors expressing gRNAs were selected in the presence of 2 μg/mL puromycin for 10 days and clonal Rab11a KO cells were generated by limiting dilution of the polyclonal population. Rab11a KO cells were identified by PCR analysis of the targeted genomic region using the following primers (forward TGTTCAACCCCCTACCCCCATTC and reverse TGGAAGCAAACACCAGGAAGAACTC) and further confirmed by western blot analysis of Rab11a expression (36).

Viruses

All viruses used in this study were generated by reverse genetics (37). For influenza A/Panama/2007/99 virus (P99; H3N2), 293T cells transfected with reverse-genetics plasmids 16–24 h previously were injected into the allantoic cavity of 9- to 11-d-old embryonated chicken eggs and incubated at 37 °C for 40–48 h. The resultant egg passage 1 stocks were used in experiments. For influenza A/Netherlands/602/2009 virus (NL09; pH1N1), 293T cells transfected with reverse-genetics plasmids 16–24 h previously were co-cultured with MDCK cells at 37 °C for 40–48 h. The supernatants were then propagated in MDCK cells at a low MOI to generate NL09 working stocks. The titers for these viruses were obtained by plaque assays on MDCK cells.

The NL09 ΔHA Venus WT, P99 ΔHA Venus WT and NL09 ΔHA Scarlet VAR viruses were generated by reverse genetics by co-culture with MDCK WSN HA cells rather than MDCK cells. The ΔHA Venus and ΔHA Scarlet rescue plasmids were prepared by inserting either the mVenus (38) or mScarlet (39) ORF within the HA sequence, retaining only the 3’ terminal 136 nucleotides of the

HA segment upstream of the reporter gene start codon and the 5' terminal 136 nucleotides of the HA segment downstream of the reporter gene stop codon. ATG sequences within the upstream portion were mutated to ATT to prevent premature translation start (40). As previously described (41), one silent mutation was introduced into each NL09 cDNA to generate the NL09 VAR reverse genetics system, which was used to generate the NL09 ΔHA Scarlet VAR virus. These silent mutations enable differentiation of VAR virus segments from those of the WT virus using high-resolution melt analysis (19,42).

Immunofluorescence and Imaging

For fixed cell imaging, MDCK, A549 WT or A549 Rab11a KO cells were seeded onto glass coverslips. Infection with either NL09 or P99 viruses was performed the next day by adding 250 µl of inoculum to the coverslips and incubating at 37°C for 1 h with intermittent rocking. Inoculum was removed, cells washed twice with 1X PBS and Opti-MEM added to the dish. After incubation at 37°C for 24 h, cells were washed with 1X PBS (Corning) thrice and fixed with 4% paraformaldehyde (AlfaAesar) for 15 minutes at room temperature. Cells were washed with 1X PBS and permeabilized using 1% Triton X-100 (Sigma) in PBS for 5 minutes at room temperature and washed with 1X PBS. Cells were stained with mouse anti NP antibody (Abcam ab43821) (1:100), rabbit anti Rab11a antibody (Sigma HPA051697) (1:100), and Phalloidin Alexa Fluor 647 (Invitrogen A22287) (1:40) overnight at 4°C. Cells were washed thrice with 1X PBS and incubated with donkey anti mouse Alexa Fluor 555 (Invitrogen A32773) (1:1000) and Anti rabbit Alexa Fluor 488 (Invitrogen A32731) (1:1000) for 1 h at 37°C.

For the A549 Rab11a KO plus A549 mCherry Rab11a co-cultures, seeding, infection, fixation and permeabilization were performed as above. Cells were stained with mouse anti NP antibody (Abcam ab43821) (1:100), and Phalloidin Alexa Fluor 647 (Invitrogen A22287) (1:40) overnight at 4°C. Cells were washed thrice with 1X PBS and incubated with donkey anti mouse Alexa Fluor 488 (Invitrogen A21202) (1:1000) for 1 h at 37°C. Cells were washed thrice with 1X PBS and once with ultra-pure water (Gibco) before mounting on glass slides using ProLong Diamond Antifade mountant containing DAPI (Invitrogen P36962). Confocal images were collected using the Olympus FV1000 Inverted Microscope at 60X 1.49 NA Oil magnification on a Prior motorized stage. Images were acquired with a Hamamatsu Flash 4.0 sCMOS camera controlled with Olympus Fluoview v4.2 software. All images were processed using Fiji image analysis software (43).

Quantification of cell-cell transmission

MDCK, A549 WT and A549 KO cells were inoculated with NL09 ΔHA Venus WT or P99 ΔHA Venus WT virus at a MOI of 0.5 PFU/cell and incubated for 1 h at 37°C. Cells were washed with 1X PBS (Corning) to remove residual inoculum and supplemented with OPTI-MEM (Gibco) without trypsin and in the presence of 30 µM Cytochalasin D (Sigma) where indicated and incubated at 37°C. Infected cells were counted by the presence of green fluorescence using an epifluorescence microscope (Zeiss) at the time points indicated and binned into single infected or foci of infected cells. Foci were defined as clusters of at least two contiguous, positive, cells. The cell counts were graphed using the GraphPad Prism software (44).

Co-culture for production of infectious virus

MDCK, A549 WT or A549 Rab11a KO cells were inoculated with either NL09 ΔHA Venus WT or NL09 ΔHA Venus VAR at a MOI of 25 PFU/cell or 2.5 PFU/cell and were incubated in virus medium without trypsin for 2 h at 37 °C. Cells were washed twice with 1X PBS (Corning) and then treated with PBS-HCl, pH 3.0 for 5 min at room temperature to remove residual inoculum. Cells were washed once with 1X PBS and then trypsinized using 0.5 M trypsin-EDTA (Corning). Cell slurry was collected in growth medium containing FBS and centrifuged at 1000 rpm or 5 minutes in a tabletop centrifuge (Thermo Sorvall ST16) to pellet cells. Supernatant was aspirated and cells resuspended in virus medium containing TPCK-trypsin (Sigma), 20 mM HEPES (Corning) and 50 mM NH_4Cl (Sigma) with or without 30 µM Cytochalasin D (Sigma) as indicated. Infected cell slurry was mixed with naïve MDCK WSN HA cells in a ratio of 1:1:2 of NL09 ΔHA Venus WT: NL09 ΔHA Scarlet VAR: Naïve MDCK WSN HA cells respectively and plated onto 6-well plates. Cells were allowed to attach at 37 °C and supernatant was collected at indicated time points for analysis.

Quantification of reassortment

Reassortment was quantified for coinfection supernatants as described previously (19). Briefly, plaque assays were performed on MDCK WSN HA cells in 10 cm dishes to isolate virus clones. Serological pipettes (1 ml) were used to collect agar plugs into 160 µl PBS. Using a ZR-96 viral RNA kit (Zymo), RNA was extracted from the agar plugs and eluted in 40 µl nuclease-free water (Invitrogen). Reverse transcription was performed using Maxima reverse transcriptase (RT; Thermofisher) according to the manufacturer's protocol. The resulting cDNA was diluted 1:4 in nuclease-free water, each cDNA was combined with segment-specific primers (Supplementary Table 1) and Precision melt supermix (Bio-Rad) and analysed by qPCR using a CFX384 Touch real-time PCR detection system (Bio-Rad) designed to amplify a region of approximately 100 bp from

each gene segment that contains a single nucleotide change in the VAR virus. The qPCR was followed by high-resolution melt analysis to differentiate the WT and VAR amplicons (19). Precision Melt Analysis software (Bio-Rad) was used to determine the parental virus origin of each gene segment based on the melting properties of the cDNA fragments and comparison to WT and VAR controls. Each plaque was assigned a genotype based on the combination of WT and VAR genome segments, with two variants on each of seven segments allowing for 128 potential genotypes.

Acknowledgements:

We thank Drs. Seema Lakdawala and Ryan Langlois for generous sharing of cell lines. This research project was supported in part by the Emory University Integrated Cellular Imaging Microscopy Core and was funded by NIH/NIAID Centers of Excellence in Influenza Research and Surveillance (CEIRS), contract number HHSN272201400004C and NIH R01AI127799. Julianna Han was partly supported by the NIH Molecular and Cellular Biology training program at The University of Chicago (T32GM007183); Julianna Han was partly supported the NIH Diversity Supplement (R01AI123359- 02S1). Dr. Balaji Manicassamy is supported by NIAID grants (R01AI123359 and R01AI127775).

References:

1. Noda T. Selective Genome Packaging Mechanisms of Influenza A Viruses. Cold Spring Harb Perspect Med. 2020;

2. Eisfeld AJ, Kawakami E, Watanabe T, Neumann G, Kawaoka Y. RAB11A Is Essential for Transport of the Influenza Virus Genome to the Plasma Membrane. J Virol. 2011;

3. Weisz OA, Rodriguez-Boulan E. Apical trafficking in epithelial cells: Signals, clusters and motors. Journal of Cell Science. 2009.

4. Chen W, Feng Y, Chen D, Wandinger-Ness A. Rab11 is required for trans-Golgi network-to-plasma membrane transport and a preferential target for GDP dissociation inhibitor. Mol Biol Cell. 1998;

5. Nturibi E, Bhagwat AR, Coburn S, Myerburg MM, Lakdawala SS. Intracellular Colocalization of Influenza Viral RNA and Rab11A Is Dependent upon Microtubule Filaments. J Virol. 2017;

6. Bhagwat AR, Le Sage V, Nturibi E, Kulej K, Jones J, Guo M, et al. Quantitative live cell imaging reveals influenza virus manipulation of Rab11A transport through reduced dynein association. Nat Commun. 2020;

7. Amorim MJ, Bruce EA, Read EKC, Foeglein A, Mahen R, Stuart AD, et al. A Rab11- and Microtubule-Dependent Mechanism for Cytoplasmic Transport of Influenza A Virus Viral RNA. J Virol. 2011;

8. Bruce EA, Digard P, Stuart AD. The Rab11 Pathway Is Required for Influenza A Virus Budding and Filament Formation. J Virol. 2010;

9. Austefjord MW, Gerdes HH, Wang X. Tunneling nanotubes: Diversity in morphology and structure. Commun Integr Biol. 2014;

10. Gerdes HH, Carvalho RN. Intercellular transfer mediated by tunneling nanotubes. Current Opinion in Cell Biology. 2008.

11. Abounit S, Zurzolo C. Wiring through tunneling nanotubes - from electrical signals to organelle transfer. J Cell Sci. 2012;

12. Marzo L, Gousset K, Zurzolo C. Multifaceted roles of tunneling nanotubes in intercellular communication. Frontiers in Physiology. 2012.

13. Hashimoto M, Bhuyan F, Hiyoshi M, Noyori O, Nasser H, Miyazaki M, et al. Potential Role of the Formation of Tunneling Nanotubes in HIV-1 Spread in Macrophages. J Immunol. 2016;

14. Bracq L, Xie M, Benichou S, Bouchet J. Mechanisms for cell-to-cell transmission of HIV-1. Frontiers in Immunology. 2018.

15. Eugenin E a, Gaskill PJ, Berman JW. A potential mechanism for intercellular HIV trafficking. Commun Integr Biol. 2009;

16. Panasiuk M, Rychłowski M, Derewońko N, Bieńkowska-Szewczyk K. Tunneling Nanotubes as a Novel Route of Cell-to-Cell Spread of Herpesviruses. J Virol. 2018;

17. Kumar A, Kim JH, Ranjan P, Metcalfe MG, Cao W, Mishina M, et al. Influenza virus exploits tunneling nanotubes for cell-to-cell spread. Sci Rep. 2017;

18. Roberts KL, Manicassamy B, Lamb RA. Influenza A Virus Uses Intercellular Connections To Spread to Neighboring Cells. J Virol. 2015;

19. Marshall N, Priyamvada L, Ende Z, Steel J, Lowen AC. Influenza Virus Reassortment

462 Occurs with High Frequency in the Absence of Segment Mismatch. PLoS Pathog. 2013;

463 20. Jansens RJJ, Tishchenko A, Favoreel HW. Bridging the Gap: Virus Long-Distance Spread
464 via Tunneling Nanotubes. J Virol. 2020;

465 21. Kimura S, Hase K, Ohno H. Tunneling nanotubes: Emerging view of their molecular
466 components and formation mechanisms. Exp Cell Res. 2012;

467 22. Zhu S, Bhat S, Syan S, Kuchitsu Y, Fukuda M, Zurzolo C. Rab11a-Rab8a cascade regulates
468 the formation of tunneling nanotubes through vesicle recycling. J Cell Sci. 2018;

469 23. Gousset K, Marzo L, Commere PH, Zurzolo C. Myo10 is a key regulator of TNT formation
470 in neuronal cells. J Cell Sci. 2013;

471 24. Sartori-Rupp A, Cordero Cervantes D, Pepe A, Gousset K, Delage E, Corroyer-Dulmont S,
472 et al. Correlative cryo-electron microscopy reveals the structure of TNTs in neuronal
473 cells. Nat Commun. 2019;

474 25. Delage E, Cervantes DC, Pénard E, Schmitt C, Syan S, Disanza A, et al. Differential identity
475 of Filopodia and Tunneling Nanotubes revealed by the opposite functions of actin
476 regulatory complexes. Sci Rep. 2016;

477 26. Horgan CP, Hanscom SR, Jolly RS, Futter CE, McCaffrey MW. Rab11-FIP3 links the Rab11
478 GTPase and cytoplasmic dynein to mediate transport to the endosomal-recycling
479 compartment. J Cell Sci. 2010;

480 27. Horgan CP, Hanscom SR, Jolly RS, Futter CE, McCaffrey MW. Rab11-FIP3 binds dynein
481 light intermediate chain 2 and its overexpression fragments the Golgi complex. Biochem

Biophys Res Commun. 2010;

28. Hales CM, Vaerman JP, Goldenring JR. Rab11 family interacting protein 2 associates with myosin Vb and regulates plasma membrane recycling. J Biol Chem. 2002;

29. Schafer JC, Baetz NW, Lapierre LA, Mcrae RE, Roland JT, Goldenring JR. Rab11-FIP2 interaction with myo5b regulates movement of rab11a-containing recycling vesicles. Traffic. 2014;

30. Lapierre LA, Kumar R, Hales CM, Navarre J, Bhartur SG, Burnette JO, et al. Myosin Vb is associated with plasma membrane recycling systems. Mol Biol Cell. 2001;

31. Kimura S, Hase K, Ohno H. The molecular basis of induction and formation of tunneling nanotubes. Cell and Tissue Research. 2013.

32. Fonville JM, Marshall N, Tao H, Steel J, Lowen AC. Influenza Virus Reassortment Is Enhanced by Semi-infectious Particles but Can Be Suppressed by Defective Interfering Particles. PLoS Pathog. 2015;

33. Jacobs NT, Onuoha NO, Antia A, Steel J, Antia R, Lowen AC. Incomplete influenza A virus genomes occur frequently but are readily complemented during localized viral spread. Nat Commun. 2019;

34. Phipps KL, Ganti K, Jacobs NT, Lee CY, Carnaccini S, White MC, et al. Collective interactions augment influenza A virus replication in a host-dependent manner. Nat Microbiol. 2020;

35. Gallagher ME, Brooke CB, Ke R, Koelle K. Causes and consequences of spatial within-host

viral spread. Viruses. 2018.

36. Han J, Perez JT, Chen C, Andrade J, Manicassamy B, Han J, et al. Genome-wide CRISPR / Cas9 Screen Identifies Host Factors Essential for Influenza Virus Replication. Cell Rep. 2018;23(2):596–607.

37. Neumann G, Watanabe T, Ito H, Watanabe S, Goto H, Gao P, et al. Generation of influenza A viruses entirely from cloned cDNAs. Proc Natl Acad Sci U S A. 1999;

38. Cox RS, Dunlop MJ, Elowitz MB. A synthetic three-color scaffold for monitoring genetic regulation and noise. J Biol Eng. 2010;

39. Bindels DS, Haarbosch L, Van Weeren L, Postma M, Wiese KE, Mastop M, et al. MScarlet: A bright monomeric red fluorescent protein for cellular imaging. Nat Methods. 2016;

40. White MC, Steel J, Lowen AC. Heterologous Packaging Signals on Segment 4, but Not Segment 6 or Segment 8, Limit Influenza A Virus Reassortment. J Virol. 2017;

41. Phipps KL, Marshall N, Tao H, Danzy S, Onuoha N, Steel J, et al. Seasonal H3N2 and 2009 Pandemic H1N1 Influenza A Viruses Reassort Efficiently but Produce Attenuated Progeny. J Virol. 2017;

42. Wittwer CT, Reed GH, Gundry CN, Vandersteen JG, Pryor RJ. High-resolution genotyping by amplicon melting analysis using LCGreen. Clin Chem. 2003;

43. Schindelin J, Arganda-Carreras I, Frise E, Kaynig V, Longair M, Pietzsch T, et al. Fiji: An open-source platform for biological-image analysis. Nature Methods. 2012.

44. Motulsky H. Analyzing Data with GraphPad Prism. PRism. 1999.

522

523 **Figure Legends:**

524 **Figure 1. IAV vRNPs associate with Rab11a within F-Actin rich TNTs.**

525 (A) MDCK cells, (B) A549 WT and (C) A549 Rab11a KO cells were mock-infected or infected with
526 NL09 or P99 viruses. Cells were stained for DAPI (blue), NP (red), Rab11a (green) and F-Actin
527 (pink). Representative images are shown with additional images in Supplementary Figure 1 (S1
528 A,B and C).

529 **Figure 2. Disruption of actin abrogates direct cell-cell transmission of infection.**

530 MDCK cells infected with NL09 ΔHA Venus WT (A) or P99 ΔHA Venus WT (B) were counted as
531 single infected cells or foci of infected cells. Significance of differences in the number of infected
532 foci between the control and Cytochalasin D treated groups was tested using 2-way ANOVA with
533 Bonferroni's correction for multiple comparisons (**** P-value <0.0001). Error bars represent
534 the standard error of three replicates within one representative experiment.

535 **Figure 3. Loss of Rab11a abrogates direct cell-cell transmission of infection.**

536 A549 WT or A549 Rab11a KO cells infected with NL09 ΔHA Venus WT (A) or P99 ΔHA Venus WT
537 (B) were counted as single infected cells or foci of infected cells. Significance of differences in the
538 number of infected foci between cell types was tested using 2-way ANOVA with Bonferroni's
539 correction for multiple comparisons (**** P-value <0.0001). Error bars represent the standard
540 error of three replicates within one representative experiment.

Figure 4. Virion-independent genome transfer leads to productive infection by an actin-dependent mechanism.

(A) Experimental workflow for MDCK, A549 WT or A549 Rab11a KO infection and co-culture with MDCK WSN HA cells (generated via BioRender.com). Plotted is the infectious virus yield from co-culture of MDCK WSN HA cells with (B) MDCK cells and (C) A549 WT cells or A549 Rab11a KO cells infected with NL09 ΔHA Venus WT and NL09 ΔHA Scarlet VAR viruses. Significance of differences between the control and Cytochalasin D treated cells or the WT and KO cells was tested using 2-way ANOVA with Bonferroni's correction for multiple comparisons (** P-value <0.01; *** P-value <0.001; ns=not significant). Error bars represent the standard error of three replicate infections (black circles). The dotted line represents the limit of detection of the plaque assay.

Figure 5. TNTs allow for bidirectional shuttling of Rab11a between cells.

A549 Rab11a KO cells infected with NL09 WT virus and co-cultured with uninfected A549 mCherry Rab11a cells (red), with or without Cytochalasin D. Cells stained for DAPI (blue), NP (green) and F-Actin (grey). Representative images are shown with additional images in Supplementary Figure 2 (S2).

Figure 6. TNTs serve as conduits for genome mixing and reassortment in a Rab11a dependent manner.

Genotypes of clonal viral isolates collected from the culture medium of NL09 ΔHA Venus WT and NL09 ΔHA Scarlet VAR virus infected A549 WT cells (left panels) or A549 Rab11a KO cells (right panels) co-cultured with MDCK WSN HA cells. Three replicate co-cultures per condition were sampled serially at the time points indicated and 21 plaque isolates were analyzed per sample.

562 The origin of the gene segments, represented by the columns in each table, is denoted by the
563 colored boxes (blue = WT and red = VAR). The segments are in order PB2, PB1, PA, NP, NA, M and
564 NS moving from left to right. The white panels indicate samples where no plaques were detected
565 (ND = not detected).

566 **Figure 7. Working model for Rab11a mediated vRNP transport across TNTs.**

567 vRNP complexes synthesized within the nucleus are exported out and form Rab11a-vRNP
568 complexes. Two potential fates of these complexes are shown - the classical assembly and egress
569 pathway for production of progeny virions and transport of these complexes via TNTs to an
570 uninfected cell. A new infection is initiated in the recipient cell, resulting in progeny virion
571 production. Generated via BioRender.com.

Fig 1

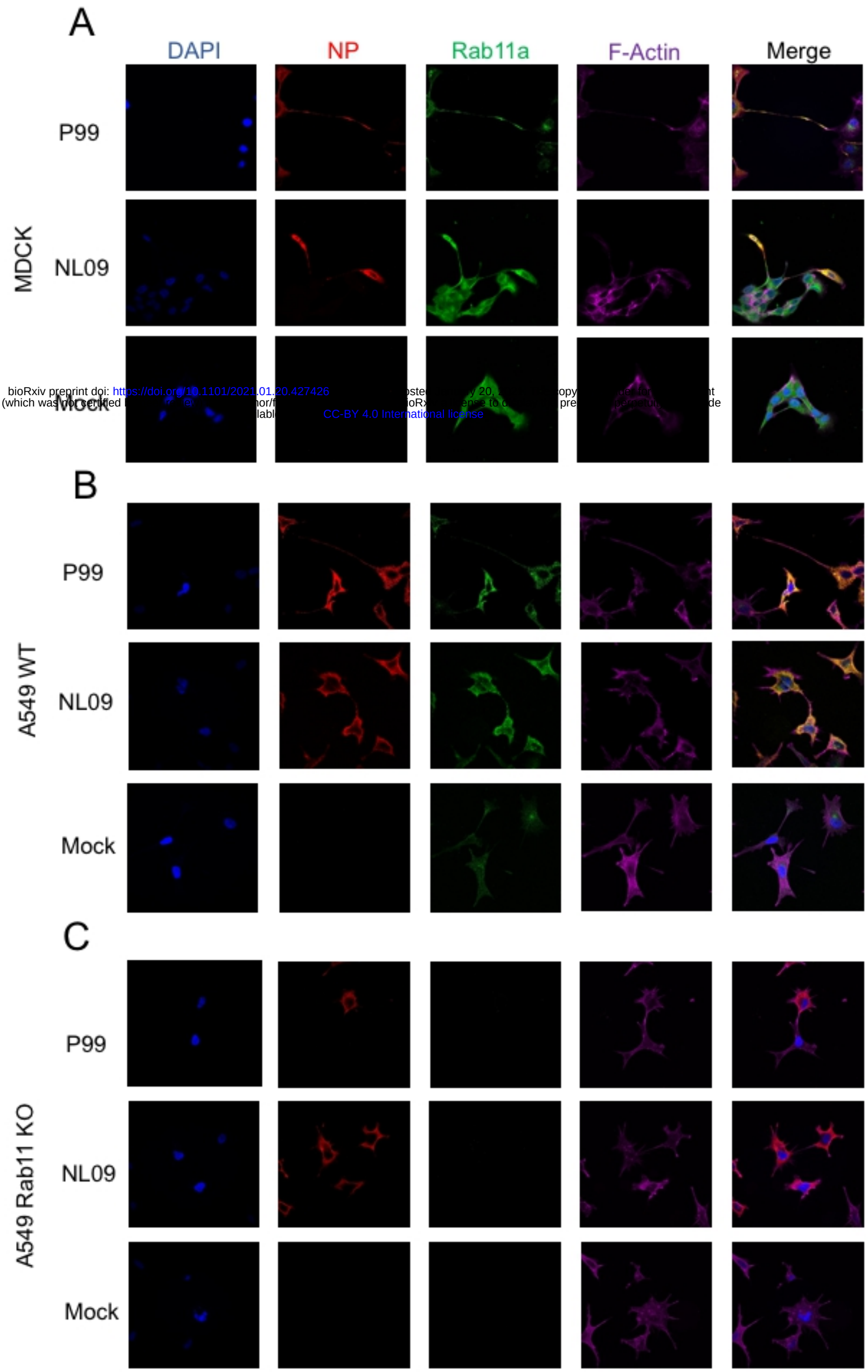

Figure 1

Fig 2

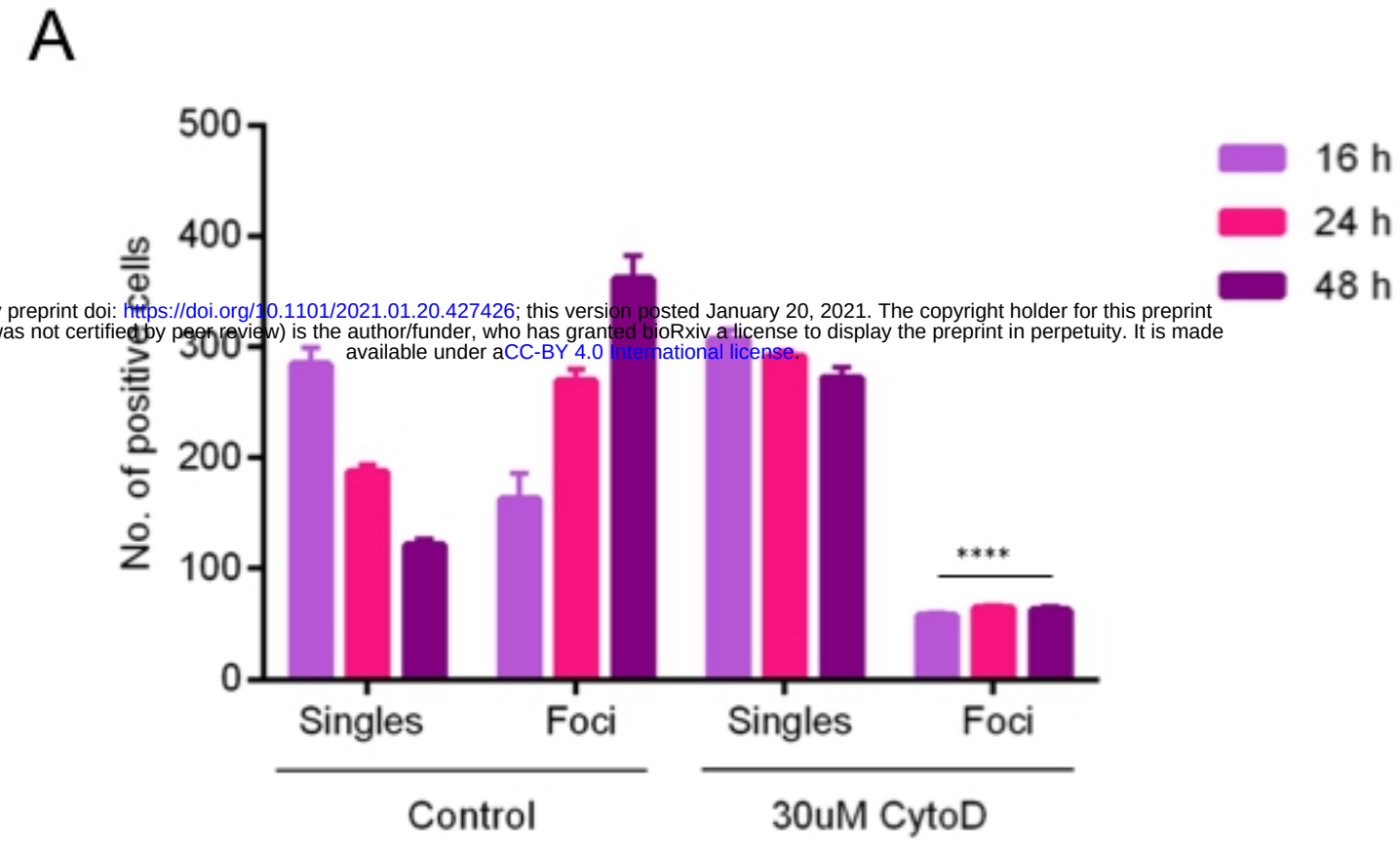

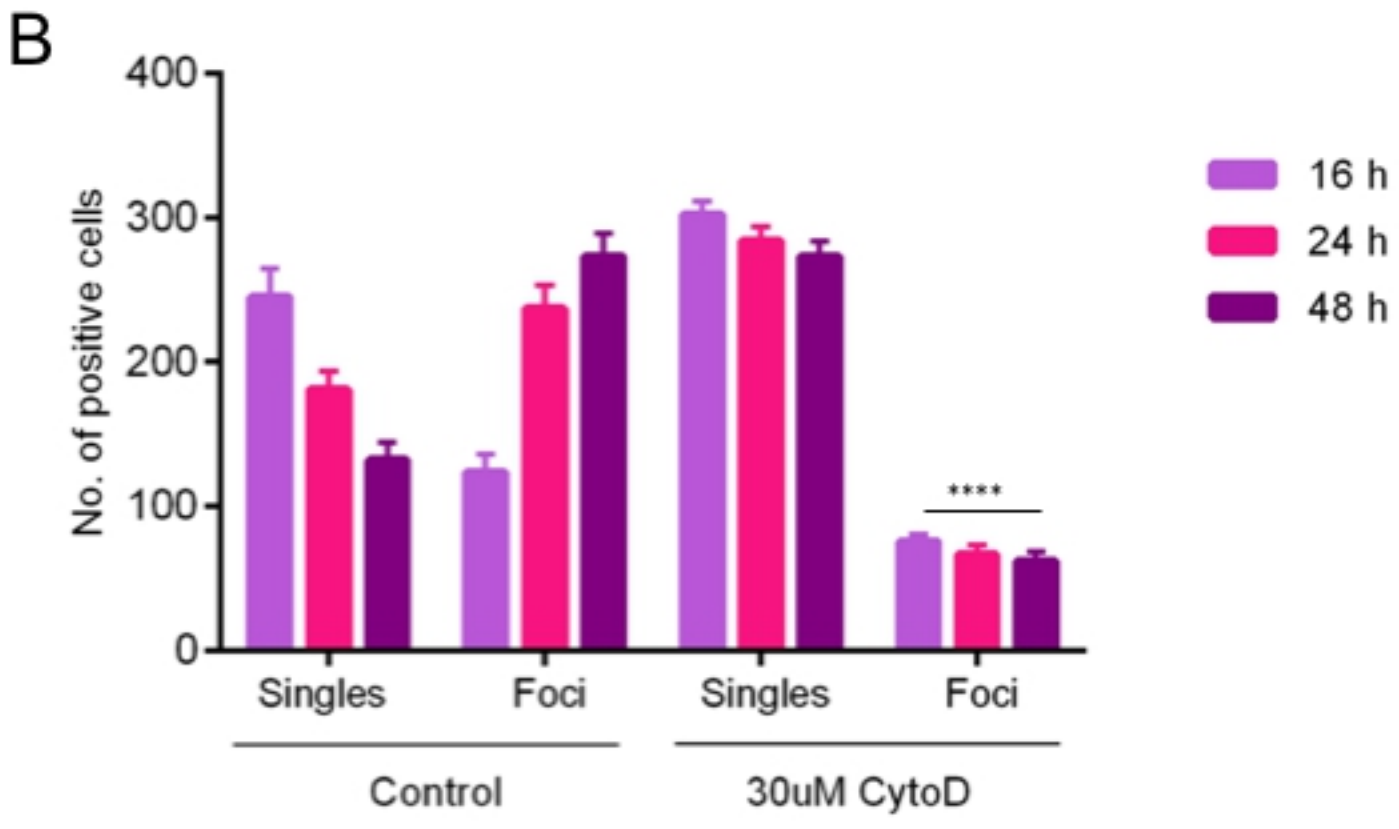

Figure 2

Fig 3

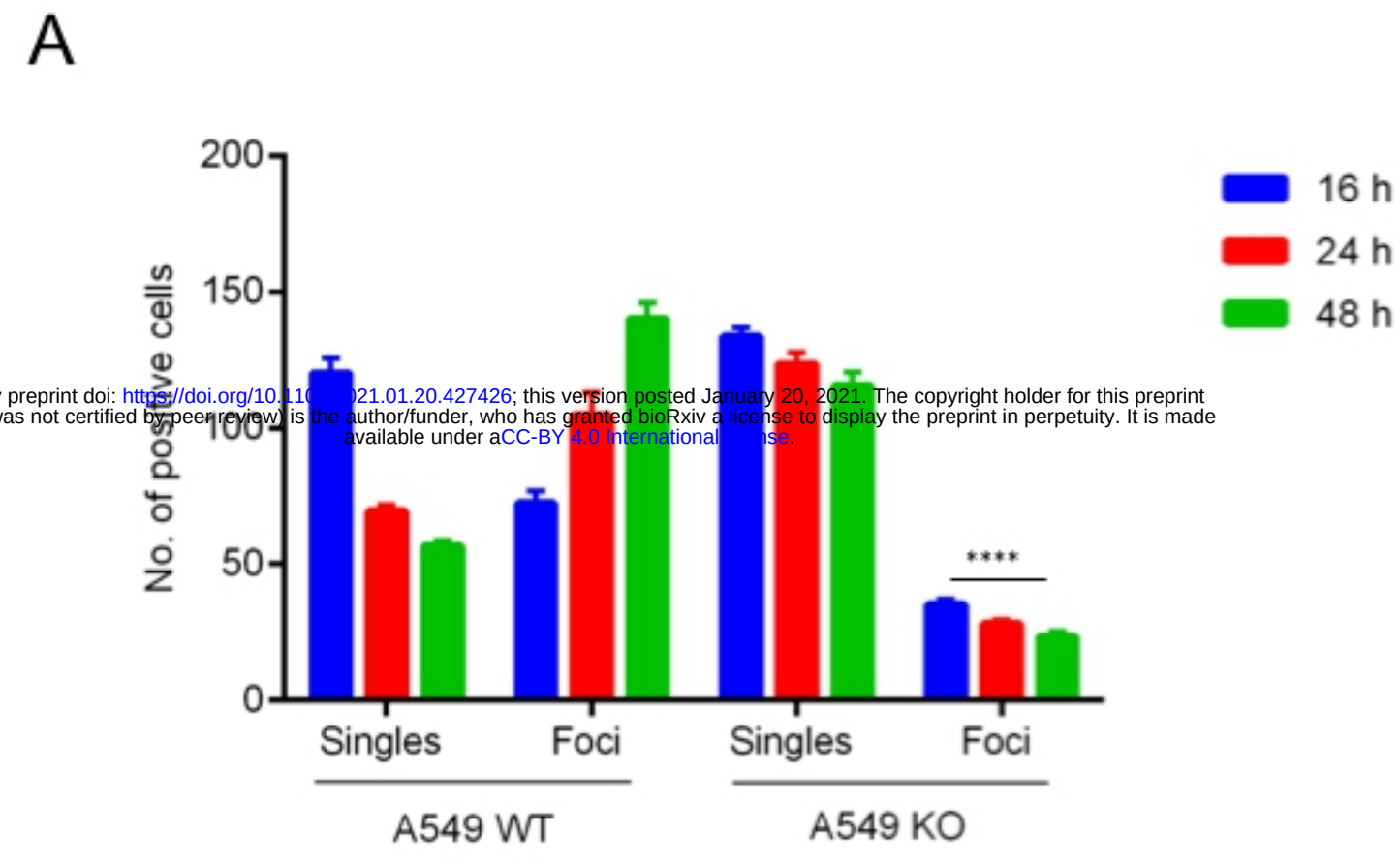

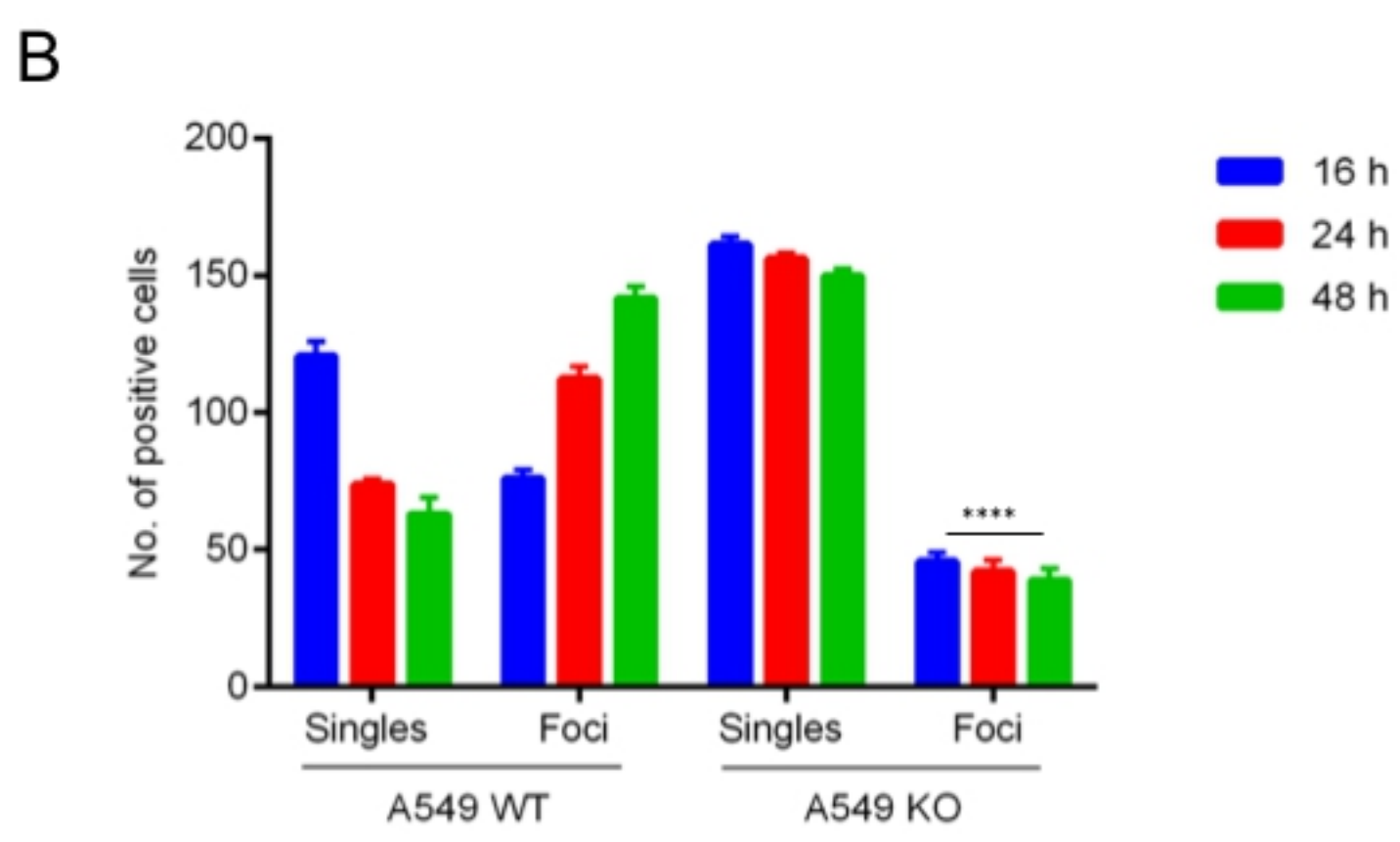

Figure 3

Fig 4

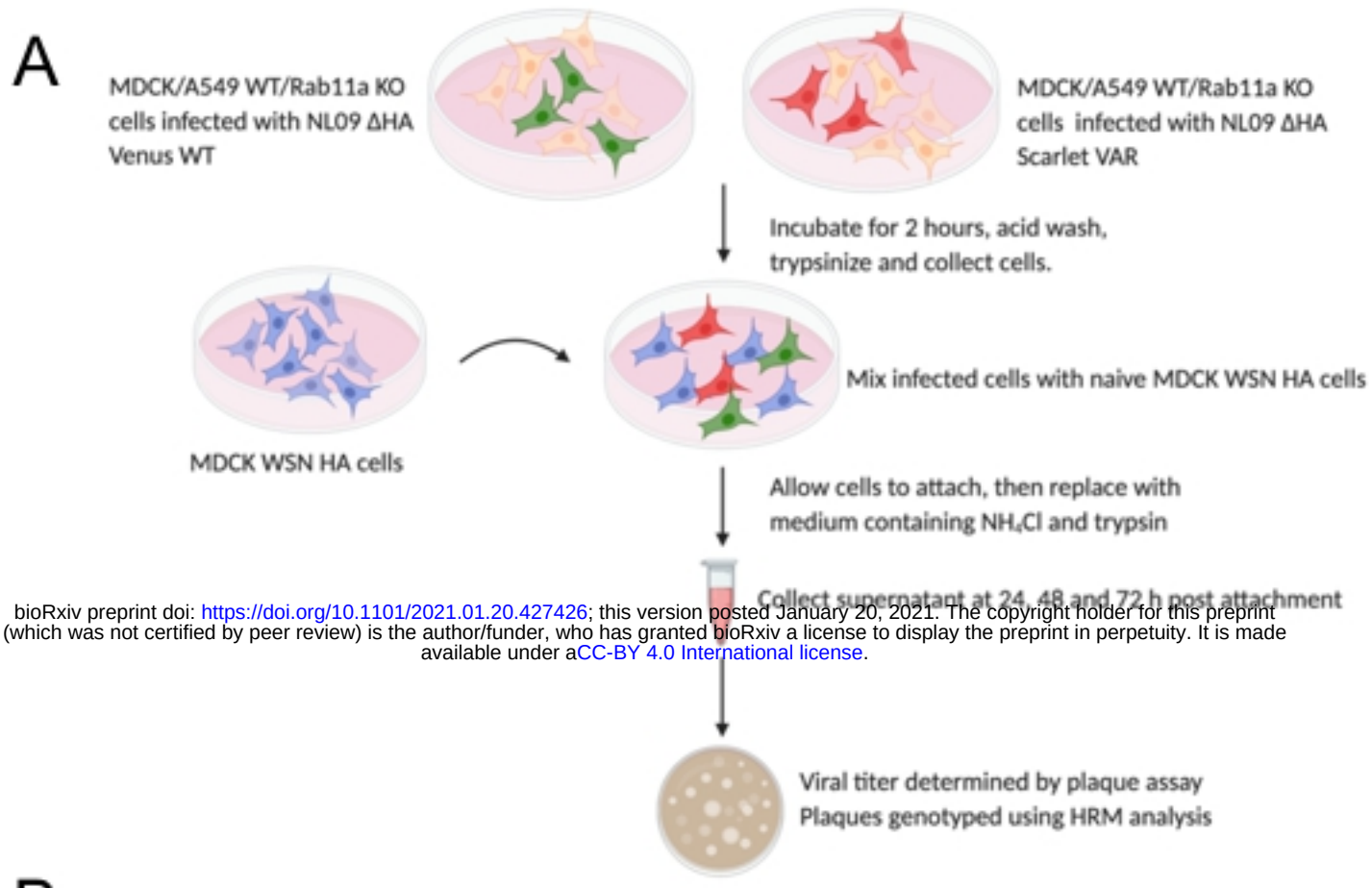

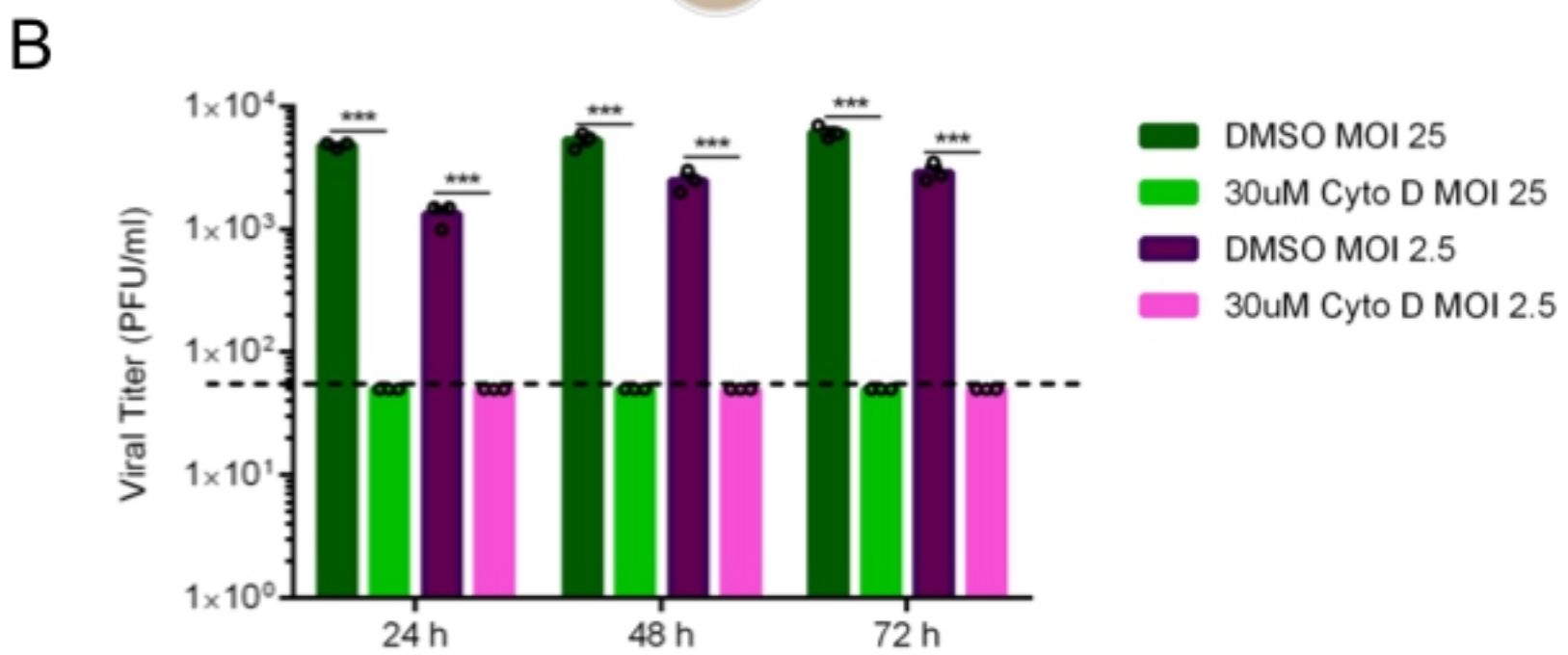

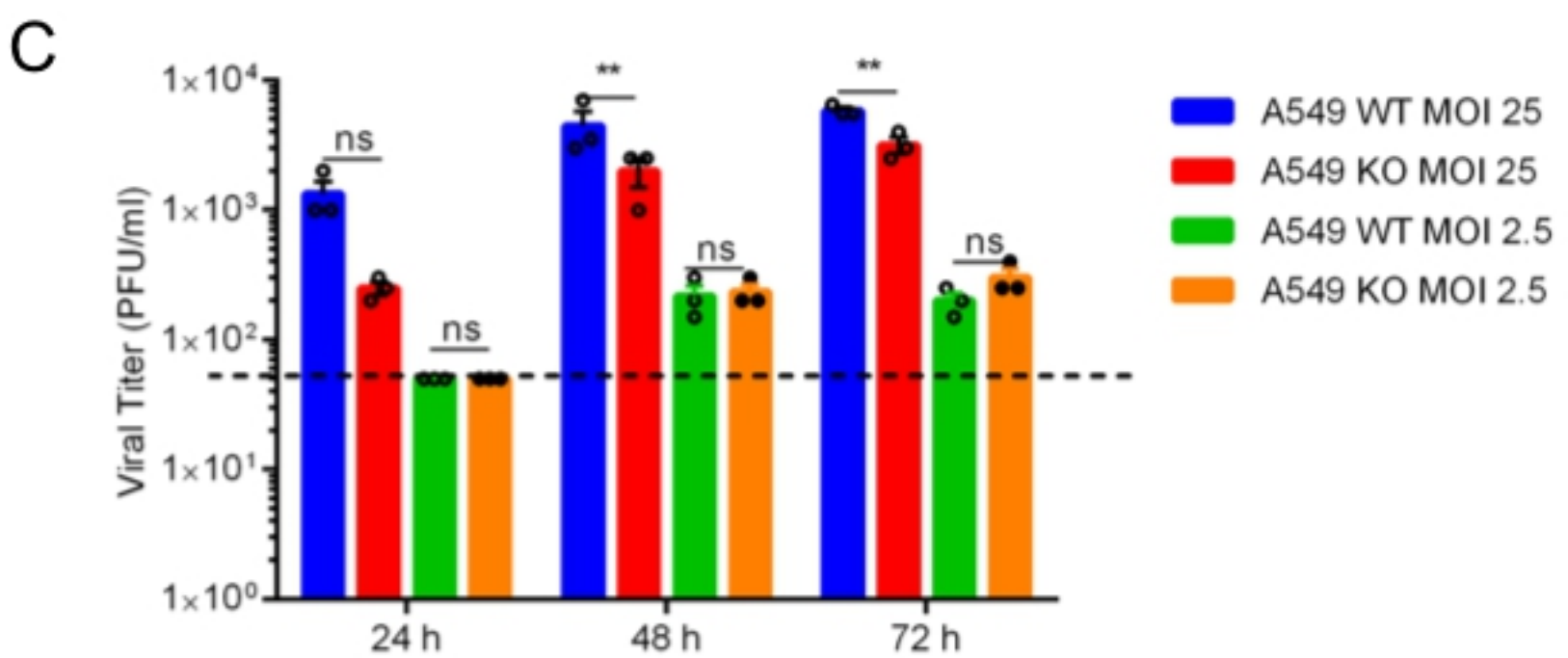

Figure 4

Fig 5

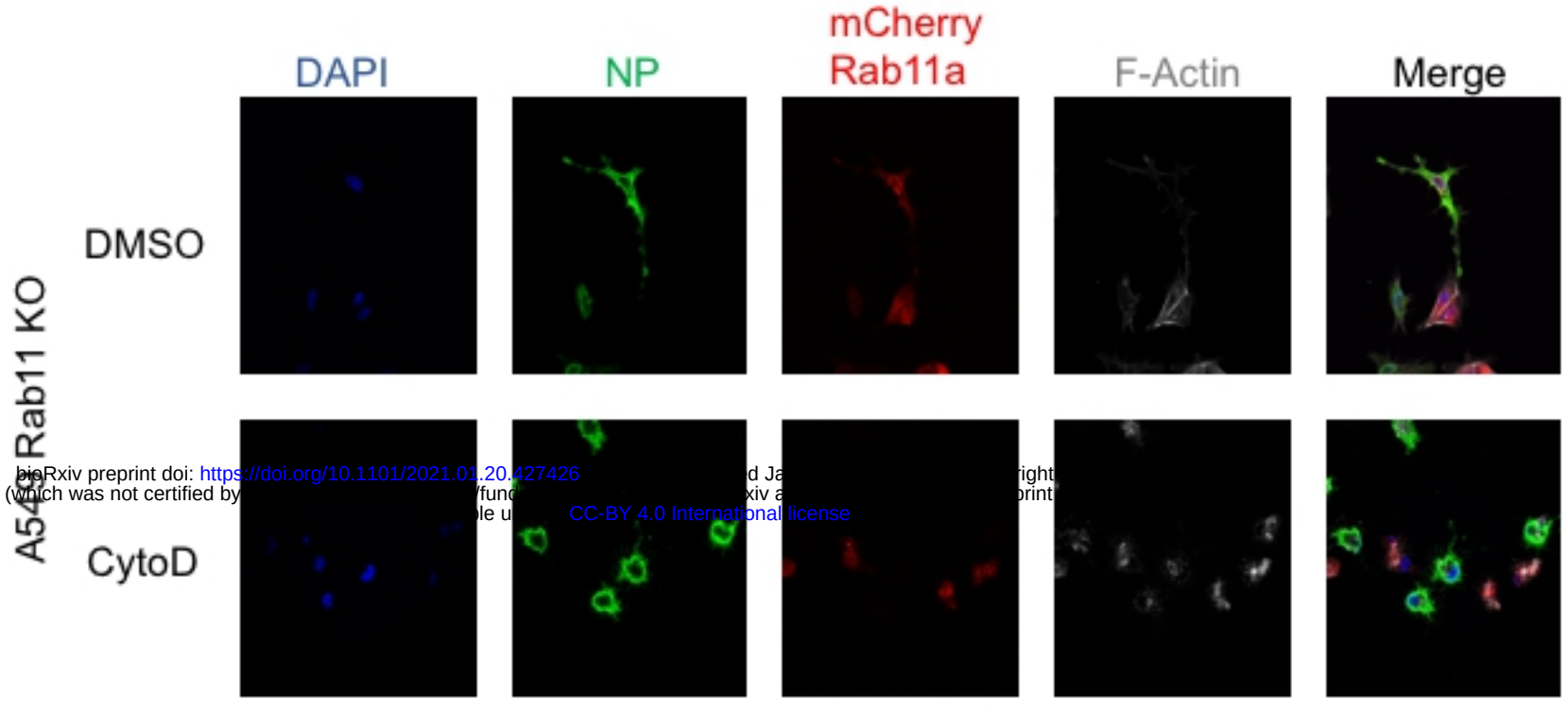

Figure 5

Fig 6

Figure 6

Fig 7

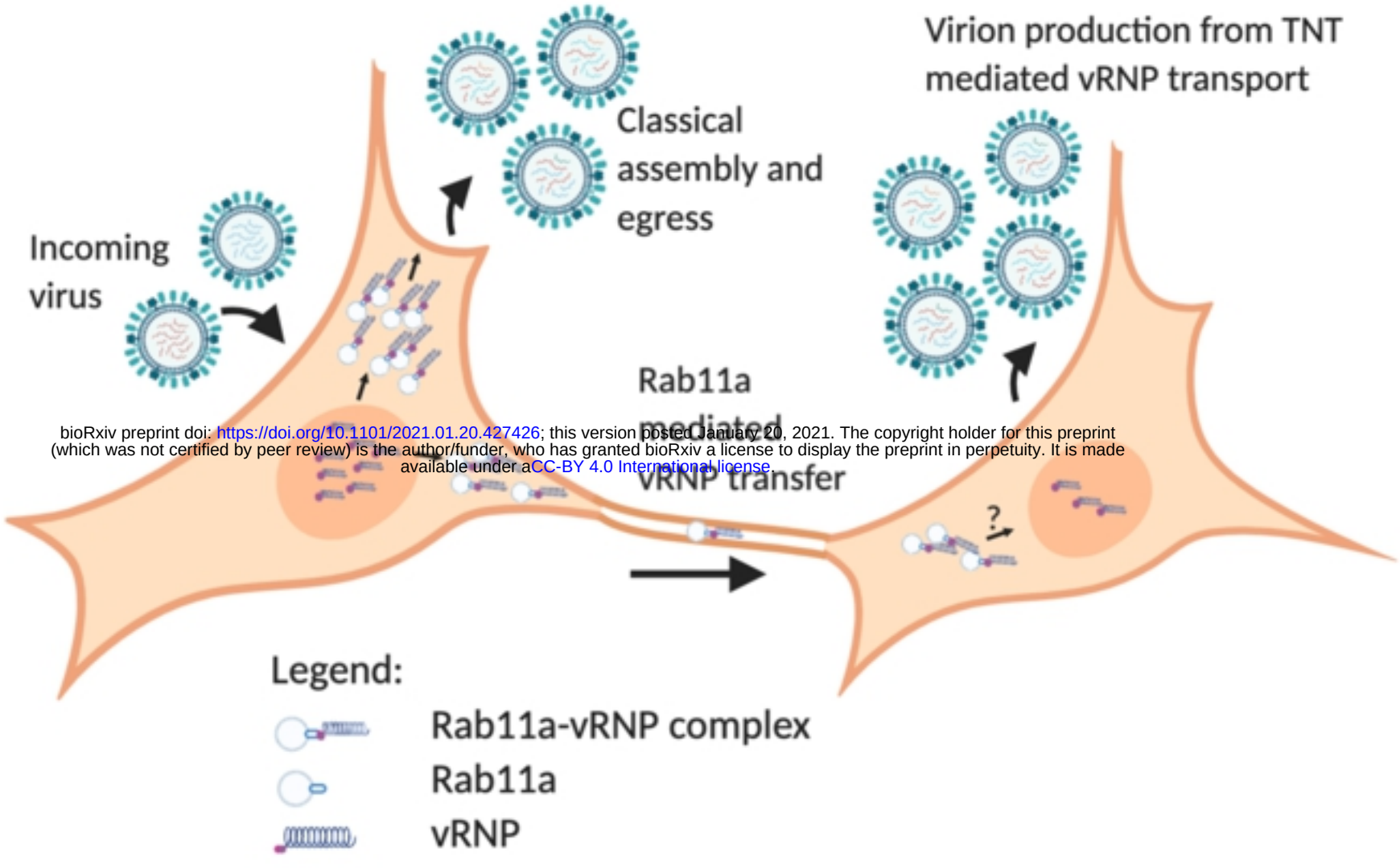

Figure 7